

Neogene faulting and volcanism in the Victoria Land Basin of the Ross Sea, Antarctica

Mei Yue^{1,2}, JinYao Gao^{1,2,3*}, ChunFeng Li^{1,4,5}, Chao Zhu^{1,2}, XinZhi Fan², Guochao Wu², ZhongYan Shen², Han Shi², XiaoXian Cai², and YiDong Guo²

¹Ocean College, Zhejiang University, Zhoushan 316021, China;

²Key Laboratory of Submarine Sciences, Second Institute of Oceanography, MNR, Hangzhou 310012, China;

³Key Laboratory of Environmental Survey Technology and Application, MNR, Guangzhou 528200, China;

⁴Sanya Institute, Zhejiang University, Sanya 572000, China;

⁵Laboratory for Marine Mineral Resources, Qingdao National Laboratory for Marine Science and Technology, Qingdao 266061, China

Key Points:

- Negative flower structures are found in the northern Terror Rift with accommodation zones.
- Two volcanic chains running through mud volcanoes in the Victoria Land basin connected three igneous provinces.
- Opposite polarities of magnetic anomalies indicate multi-phases of volcanic activities.

Citation: Yue, M., Gao, J. Y., Li, C. F., Zhu, C., Fan, X. Z., Wu, G. C., Shen, Z. Y., Shi, H., Cai, X. X., and Guo, Y. D. (2022). Neogene faulting and volcanism in the Victoria Land Basin of the Ross Sea, Antarctica. *Earth Planet. Phys.*, 6(3), 248–258. <http://doi.org/10.26464/epp2022023>

Abstract: The Neogene Terror Rift in the Antarctic Victoria Land Basin (VLB) of the Ross Sea, Antarctica, is composed of the Discovery Graben and the Lee Arch. Many Neogene volcanoes are aligned in the north-south direction in the southern VLB, belonging to the McMurdo Volcanic Group. However, due to multiple glaciations and limited seismic data, the volcanic processes are still unclear in the northern VLB, especially in the Terror Rift. Multichannel seismic profiles were collected at the VLB from the 32nd Chinese National Antarctic Research Expedition (CHINARE). We utilized four seismic profiles from the CHINARE and additional historical profiles, along with gravity and magnetic anomalies, to analyze faults and stratigraphic characteristics in the northern Terror Rift and volcanism in the VLB. Negative flower structures found in the northern Terror Rift suggest that the Terror Rift was affected by dextral strike-slip faults extending from the northern Victoria Land (NVL). After the initial orthogonal tension, the rift transitioned into an oblique extension, forming a set of downward concaving normal faults and accommodation zones in the Terror Rift. On the Lee Arch, several imbricated normal faults formed and converged into a detachment fault. Under gravitational forces, the strata bent upward and formed a rollover anticline. Many deep faults and thin strata subjected to erosion facilitated volcanic activity. A brittle volcanic region in the VLB was affected by dextral strike-slip movements and east-west extension, resulting in two Neogene volcanic chains that connect three igneous provinces in the VLB: the Hallett, Melbourne, and Erebus Provinces. These two chains contain mud volcanoes with magnetic nuclei, volcanic intrusions, and late-stage volcanic eruptions. Volcanisms have brought about opposite polarities of magnetic anomalies in Antarctica, indicating the occurrence of multiple volcanic activities.

Keywords: Victoria Land Basin; Terror Rift; seismic stratigraphy; gravity and magnetic modeling; faulting; Neogene volcanic intrusion

1. Introduction

The West Antarctic Rift System (WARS) formed from 105 to 80 Ma with the breakup of the Gondwana supercontinent (Fielding et al., 2006; Rossetti et al., 2006; Harry and Anoka, 2007). The WARS passes through the entire Ross Sea Basin and extends beneath the Ross Ice Shelf (Figure 1). The formation and evolution of the Ross Sea Basin accompanied basin depression, faulting, and volcanic activities. The Coulman High and the Central High divide the Ross Sea Basin into four main subbasins: Northern Basin, Victoria Land

Basin (VLB), Central Trough, and Eastern Basin (Cooper et al., 1987).

The Terror Rift, the central part of the VLB, marks the latest episode of WARS extension, characterized by an abnormally high heat flow (Shapiro and Ritzwoller, 2004) and thin crust (Trey et al., 1999; Pappa et al., 2019). Its internal multi-stages of extension and rifting provide channels for volcanic intrusions and eruptions. To date, many studies have been conducted on the structural characteristics of the southern Terror Rift (Hall et al., 2007; Henrys et al., 2008; Blocher, 2017; Fielding, 2018; Sauli et al., 2021), but the northern Terror Rift has been severely eroded by multiple glaciations and lacks seismic and multibeam data. Faulting in the northern Terror Rift and the distribution of volcanoes in the VLB

Correspondence to: J. Y. Gao, gaojy@sio.org.cn
Received 24 OCT 2021; Accepted 11 FEB 2022.
Accepted article online 11 APR 2022.
©2022 by Earth and Planetary Physics.

can deepen the understanding of the dynamic mechanism of the Terror Rift and the complicated evolution processes of WARS. It will also help to realize the relationship between the rupture stage transition and the driving force transformation of the Gondwana continent.

The VLB has undergone two stages of rifting. The initial rifting was associated with the rupture of the Gondwana continent, at approximately 100 Ma, and the main rifting stage began at 34 Ma (Davey and Santis, 2006). During the main rifting and subsidence of the Terror Rift, volcanism resumed in the southern VLB (Cooper et al., 1987; Fielding et al., 2008; Henrys et al., 2008). The Terror Rift is bounded by Mt. Melbourne to the north and by Mt. Erebus on the Ross Island to the south. The rift consists of the Discovery Graben, with sediments up to 14 km in thickness, and an anticline, the Lee Arch (Cooper et al., 1987; Salvini et al., 1997). The Terror Rift is stretched east to west, forming a conical rift ~350 km long and ~75 km wide in the middle that narrows to 40 km to the south and possibly extends to the interior of the northern Victoria

Land (NVL) in the north (Figure 1; Hall et al., 2007). High-angle normal faults developed on both sides of the Terror Rift with opposite dips, striking nearly north-south or northwest-southeast (Blocher, 2017).

Fully developed faults are mostly appearing near the Drygalski Ice Tongue, but not clear in the Terror Rift because of glacial erosion in the Drygalski Basin and volcanism at the ends of the rift. These north-south trending faults are discontinuous and form an eastward offset of ~25 km, appearing as accommodation zones (Hall et al., 2007), which may induce dextral strike-slip faults (Figure 1; Salvini and Storti, 1999). Dextral northwest-southeast trending strike-slip faults extend from the continental margin to NVL and limit the Neogene east-west extension of the Ross Sea Basin, forming pull-apart basins and negative flower structures. Deformation associated with the dextral strike-slip faults can be related to the crustal rheology in a brittle volcanic region (Salvini et al. 1997). The western VLB is part of the brittle volcanic region, where massive Neogene volcanoes developed at the intersection of the

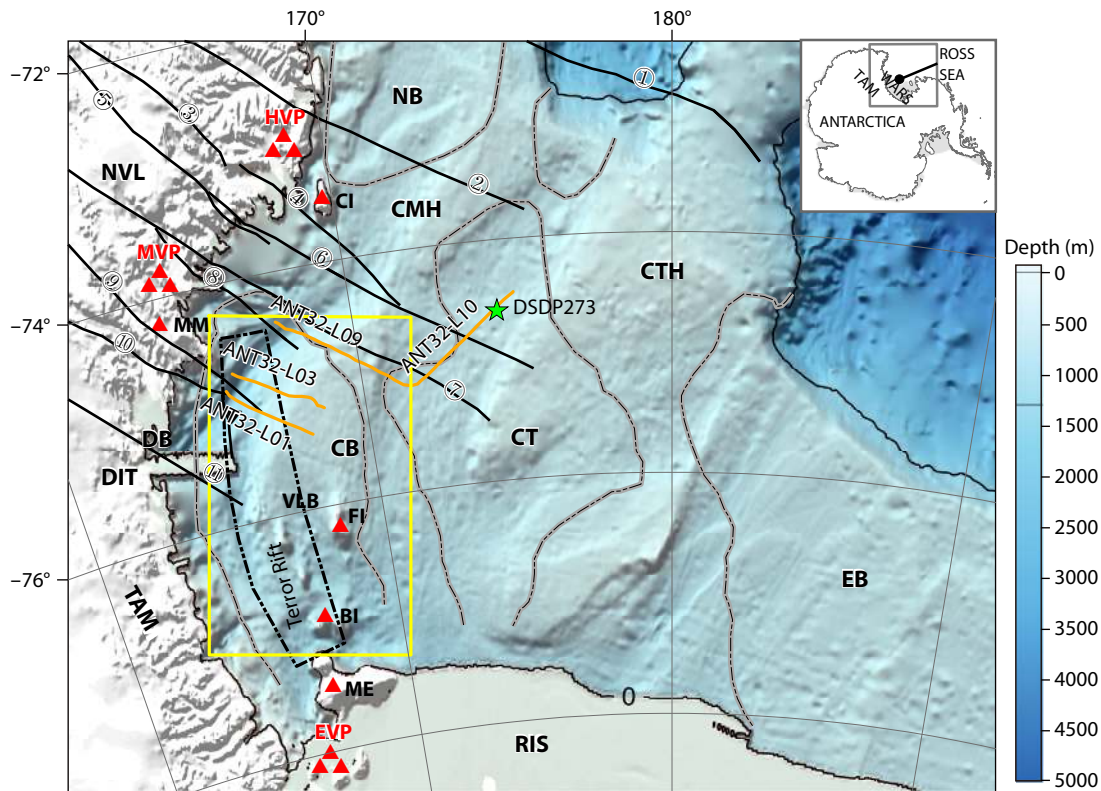


Figure 1. Bathymetric map of the Ross Sea Basin. The West Antarctic Rift System (WARS) encompasses the Ross Sea Basin and is bounded by the Transantarctic Mountains (TAM). The black box in the inset shows the location of the map. The gray dash-dotted lines mark the main structural highs and basins (Salvini et al., 1997). VLB, Victoria Land Basin; CT, Central Trough; NB, Northern Basin; EB, Eastern Basin; CMH, Coulman High; CTH, Central High; DB, Drygalski Basin; CB, Cray Bank (DB and CB are based on the definition of bathymetric terrain); DIT, Drygalski Ice Tongue; FI, Franklin Island; BI, Beaufort Island; CI, Coulman Island; MM, Mt. Melbourne; ME, Mt. Erebus; RIS, Ross Ice Shelf. The solid black line represents the coastline, and the yellow rectangle shows the study area of the Terror Rift. The single red triangle represents the location of the volcanic island while the triple triangles represent the igneous provinces belonging to the McMurdo Volcanic Group—Erebus Volcanic Provinces (EVP), Melbourne Volcanic Provinces (MVP), and Hallett Volcanic Provinces (HVP). The green star represents the borehole at site DSDP273. The thick black lines represent the main dextral strike-slip faults from Northern Victoria Land (NVL): (1) Cape Adare Fault, (2) Tucker Fault, (3–4) Leap Year Fault, (5–6) Lanterman Fault, (7–8) Aviator Fault, (9) Campbell Fault, (10) Priestley Fault, and (11) David Fault. Mt. Melbourne is located along the Campbell Fault. Four seismic profiles from the 32nd CHINARE are shown in the northern VLB. Bathymetric data are from the high-resolution digital model of the Ross Sea depth, with an interval of 250 m (Xu et al., 2018).

northwest-southeast trending faults and north-south trending faults (Cooper et al., 1987; Salvini and Storti, 1999).

Since 8 Ma, the western Ross Sea Basin has experienced a period of extensive volcanic activity. In the southern VLB, and especially in the Terror Rift, the McMurdo Volcanic Group is exposed at the foot of the Transantarctic Mountains (TAM) (Ji et al., 2017) and is still active (Kyle, 1990). Volcanoes of the McMurdo Volcanic Group occurred in four volcanic provinces, the Balleny, Hallett, Melbourne, and Erebus Provinces, and Neogene volcanoes are concentrated in the coastal area of the VLB, showing a north-south trend (Kyle and Cole, 1974). Volcanic activities in the Terror Rift mainly formed intrusions, which trend nearly north-south and increase in intensity toward the south. The ages of volcanoes are nonuniform but fall mostly in the Pleistocene (Rilling et al., 2009). The VLB was intruded by north-south trending volcanoes and turned into partially uplifted and tilted blocks (Salvini et al., 1997). The VLB can be divided into four structural belts oriented in the north-south direction. The second structural belt (i.e., the Terror Rift) and the fourth structural belt (i.e., the Coulman High) are intrusive structural belts related to late rifting (Cooper et al., 1987). Many volcanoes are found in the brittle volcanic region, but their distribution is not well delineated because of inadequate seismic data and serious denudation of glaciers in the northern VLB.

High-resolution multibeam data show pockmarks and mounds in the southern VLB, with diameters of ~400–4,000 m and heights of ~50–250 m (Magee, 2011). The existence of bottom-simulating reflectors (BSRs) confirms that some pockmarks and mounds in the southern Terror Rift developed along with submarine gas hydrates (Geletti and Buseti, 2011). According to gravity and magnetic modeling, most submarine mounds between the Lee Arch (east of the Terror Rift) and Franklin Island are volcanogenic and erupted under the ice sheet (Lawver et al., 2012).

In this study, we used new geophysical data collected in the northern Terror Rift during the 32nd Chinese National Antarctic Research Expedition (CHINARE), historical multichannel seismic (MCS) data (Brancolini et al., 1995; Fielding et al., 2008), and borehole data from Deep Sea Drilling Project Site 273 (Hayes et al., 1975) to better investigate structural characteristics of the northern Terror Rift and volcanic distributions in the VLB.

2. Dataset and Methods

The MCS data profiles ANT32-L01, ANT32-L03, ANT32-L09, and ANT32-L10 are from the 32nd CHINARE, and NBPO401-148, L284AN-407, IT90AR-63S, and IT90AR-65S are from the Antarctic Seismic Data Library System (SDLS). NBP9407-51 is not included in SDLS and is from Henrys et al. (2008). The 32nd CHINARE deployed a 210 cubic inch airgun source and a 24-channel cable with a receiver spacing of 12.5 m and a shot interval of 13 s, in an average ship speed of 5 knots. The MCS data used has a total length of 701 km.

Profiles ANT32-L01 and ANT32-L03 are located in the northern VLB and partially pass through the Terror Rift, the Drygalski Basin, and the Cray Bank. Profile ANT32-L09 partially passes through the VLB and the Coulman High (Figure 2). Profile ANT32-L10 passes through site DSDP273 in the Central Trough (Figures 1 and 3;

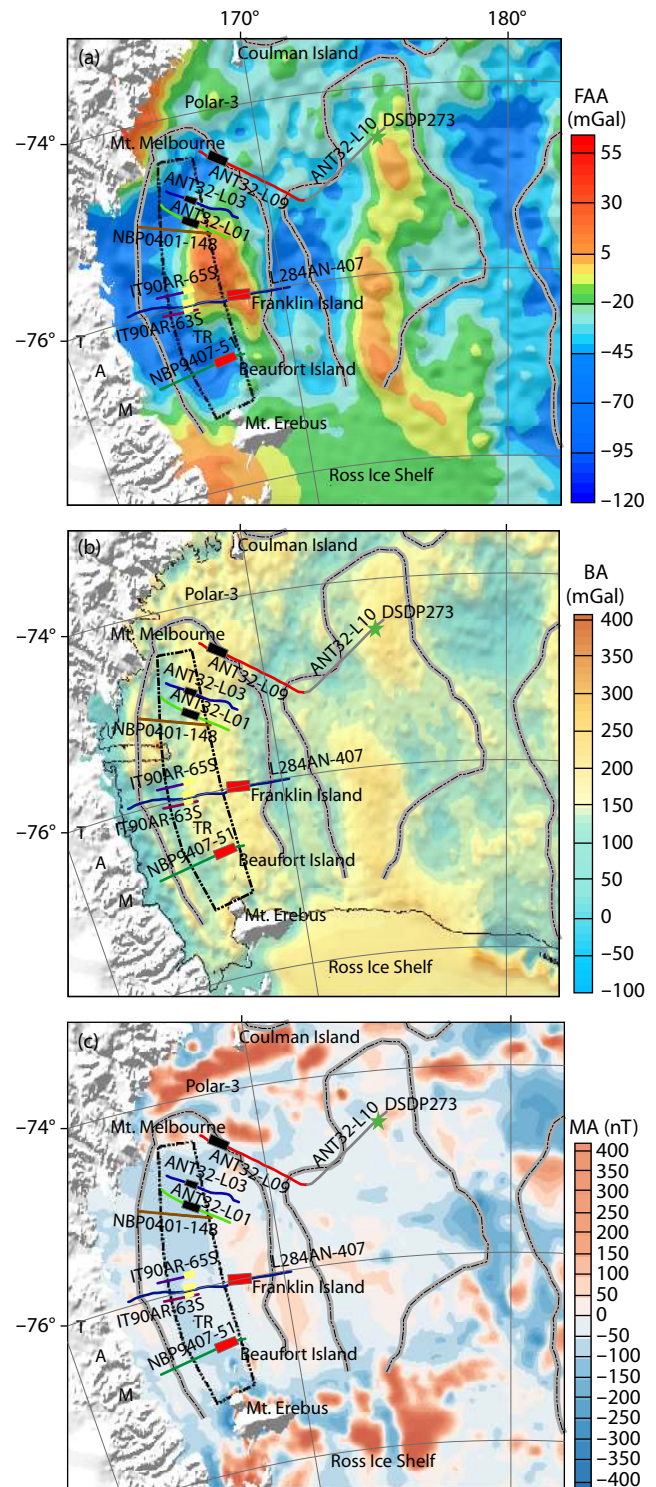


Figure 2. Gravity and magnetic anomaly maps in the western Ross Sea. (a) Free-air gravity anomaly map; (b) Bouguer gravity anomaly map; (c) Magnetic anomaly map. TR, Terror Rift; TAM, Transantarctic Mountains. Seismic profiles are from the 32nd CHINARE and SDLS. The yellow boxes represent the locations of mud volcanoes on profiles IT90AR-63S, IT90AR-65S, and L284AN-407. The red boxes represent a region of igneous volcanoes in the southern Terror Rift on profiles NBP9407-51 and L284AN-407. Polar-3 represents a large-scale igneous intrusion at 48–34 Ma.

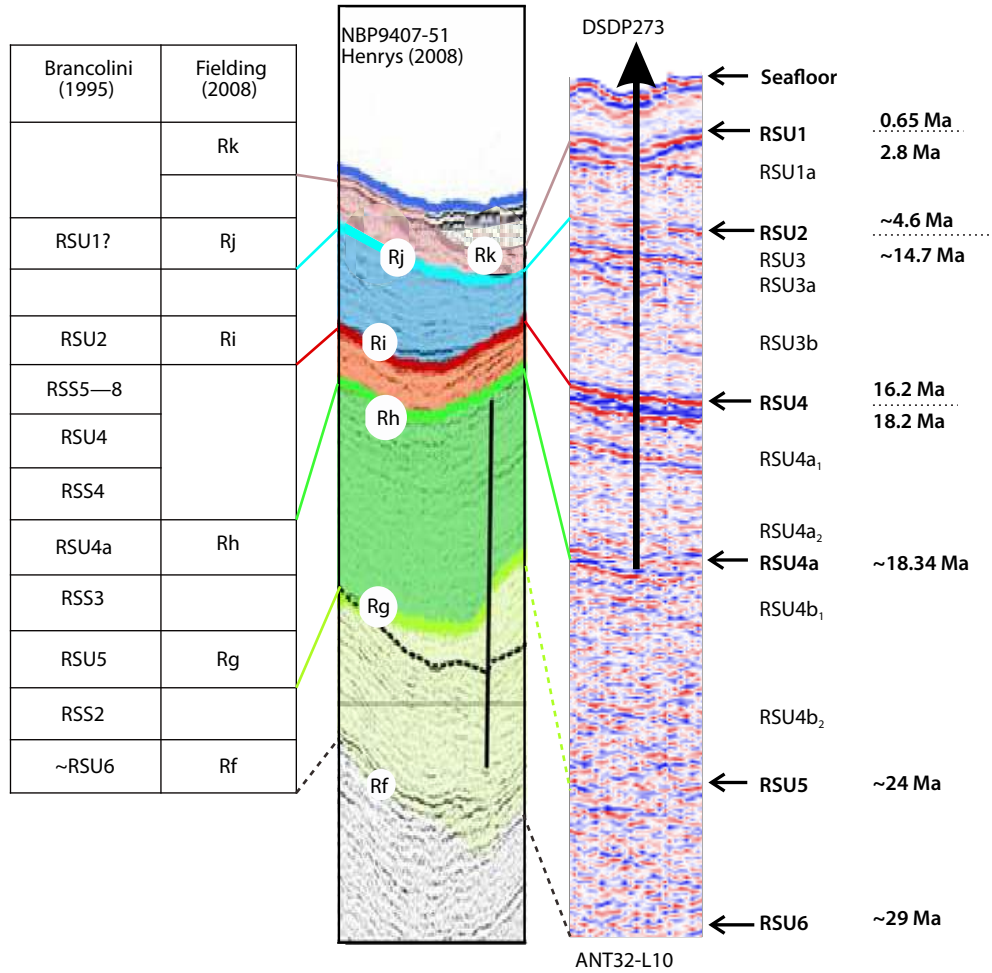


Figure 3. A new geologic time scale of stratigraphic unconformities in the VLB. TWT, two-way travel time; RSS, Ross Sea strata; RSU, Ross Sea unconformity. Profile ANT32-L10 passes through site DSDP273. This table aims to calibrate the stratigraphic age of the 32nd CHINARE seismic profile on the basis of previous studies (Brancolini et al., 1995; Fielding et al., 2008; Henrys et al., 2008).

Hayes et al., 1975). Site DSDP273 calibrates seismic interpretation of the northern VLB, whereas the interpretation in southern VLB is based on data from the Antarctic Drilling Program (ANDRILL) near Mt. Erebus (Talarico and Sandroni, 2011). Profile NBP0401-148 crosses over the whole structure of the Terror Rift, and profiles NBP9407-51, L284AN-407, IT90AR-63S, and IT90AR-65S pass through the mud volcanoes and volcanic regions in the VLB (Figure 2).

The gravity anomaly data in the study area were compiled from CRYOSAT, ENVISAT, and JASON-1 satellite altimetry data, with a grid interval of 1'x1' and an accuracy better than 1.5 mGal (Sandwell et al., 2014). The integrated magnetic anomaly grid, ADMAP, has a grid interval of 5 kmx5 km (Golynsky et al., 2006). The ice elevation and under-ice topographic data with a grid interval of 1'x1' were from the National Oceanic and Atmospheric Administration, USA. The bathymetry map of the Southern Ocean can be up to a grid interval of 500 mx500 m. According to the bathymetric map in the northern VLB, the Drygalski Basin has been affected by multi-stages of glaciations and has developed a trough with a nearly northeast trend and a water depth of more than 1,000 m. The high-terrain Cray Bank is located partly in the VLB and partly in Coulman High, where the shallowest water

depth reaches 250 m (Kooyman et al., 2020).

3. Seismic Interpretation in the Northern VLB

3.1 Stratigraphic Sequence

The seismic faces in the VLB are explicated from the stratigraphic sequence and from boreholes in the Ross Sea Basin on the basis of previous studies (Brancolini et al., 1995; Fielding et al., 2008). Borehole DSDP273 has a total penetration of 346.5 m, with a low recovery (Figure 3). The stratigraphic sequence of borehole DSDP273 contains four main unconformities: at 0.8 m in the Late Pleistocene (2.8–0.65 Ma), at 42.5 m in the Miocene (14.7–4.6 Ma), at 272.5 m in the early Miocene (18.2–16.2 Ma), and at 346.5 m (18.34 Ma; Hayes et al., 1975). The bottom of the borehole may correspond to the Ross Sea unconformity (RSU4a) (Brancolini et al., 1995), and the strata below the RSU4a are described according to the boreholes from ANDRILL (Fielding et al., 2008; Sauli et al., 2021). The oldest unconformity in the study area, RSU6 (~29 Ma), crops out only in the Drygalski Basin (Figure 3), presumed to be the basement of the Coulman High, and marks the thermal subsidence stage of the VLB (Davey and Santis, 2006). The upper Oligocene to lower Miocene section between RSU6 and RSU5

(29–24 Ma) is thicker in the Drygalski Basin than in the Crary Bank. Spatially, from ANT32-L01 through ANT32-L03 to ANT32-L09 (Figure 4), the strata gradually thicken and become sub-horizontal. The sedimentation rate increases toward the center of the Terror Rift, whereas glacial erosion is weakened in the northeast.

The sequence between RSU5 and RSU4a (24–18 Ma) developed with thermal subsidence of the VLB is undeformed, subparallel, and well layered. This section has more obvious chaotic wedges and thicker sediments deposited rapidly by glacial drift in the Drygalski Basin. RSU4 (~16 Ma) is a regional unconformity, and the sediment thickness between RSU5 and RSU4 varies greatly. Profile ANT32-L01 in the Lee Arch shows a series of normal faults forming an uplift structure, eroded at unconformity RSU2 (~4.6 Ma) (Figure 5). The local uplift of the western side of the Crary Bank, composed of the Terror Rift shoulder and excluding volcanic intrusion, indicates tectonic events related to rollover anticlines.

3.2 Faulting

The Terror Rift seems to be orthogonal and unaffected by strike-slip faults, given that strike-slip movement has not yet been found

in seismic profiles (Hall et al., 2007; Blocher, 2017). Profile ANT32-L01 (Figure 5) shows that faults with negative flower structures in the Terror Rift may be related to the dextral slip. In such a case, convergent and discrete strike-slips often appear at bends. Discontinuous and imbricated secondary faults are formed with the dislocation of the strata and are limited by the main strike-slip faults, appearing as a flower structure on the seismic profiles (Bayasgalan et al., 1999). As long as strike-slip faults cause a weakened caprock folding and slipping, a negative flower structure can be formed (Bayasgalan et al., 1999; Massironi and Kim, 2014). The flower structures discovered are asymmetric and not fully developed in the Terror Rift. A series of torsional faults occur toward one side of the backbone faults to form asymmetric inclined fault blocks. The derived torsional faults have small dips and converge downward to the backbone faults of the strike-slip structure. The negative flower structures have experienced denudation, and the superposition of the west-east extension has made the residual part difficult to observe in seismic profiles. Flower structures on profile ANT32-L01 may have been developed before RSU5 (~24 Ma) and may have terminated at RSU4a (~18.38 Ma). The Terror Rift is perhaps not a pure orthogonal rift but may have experi-

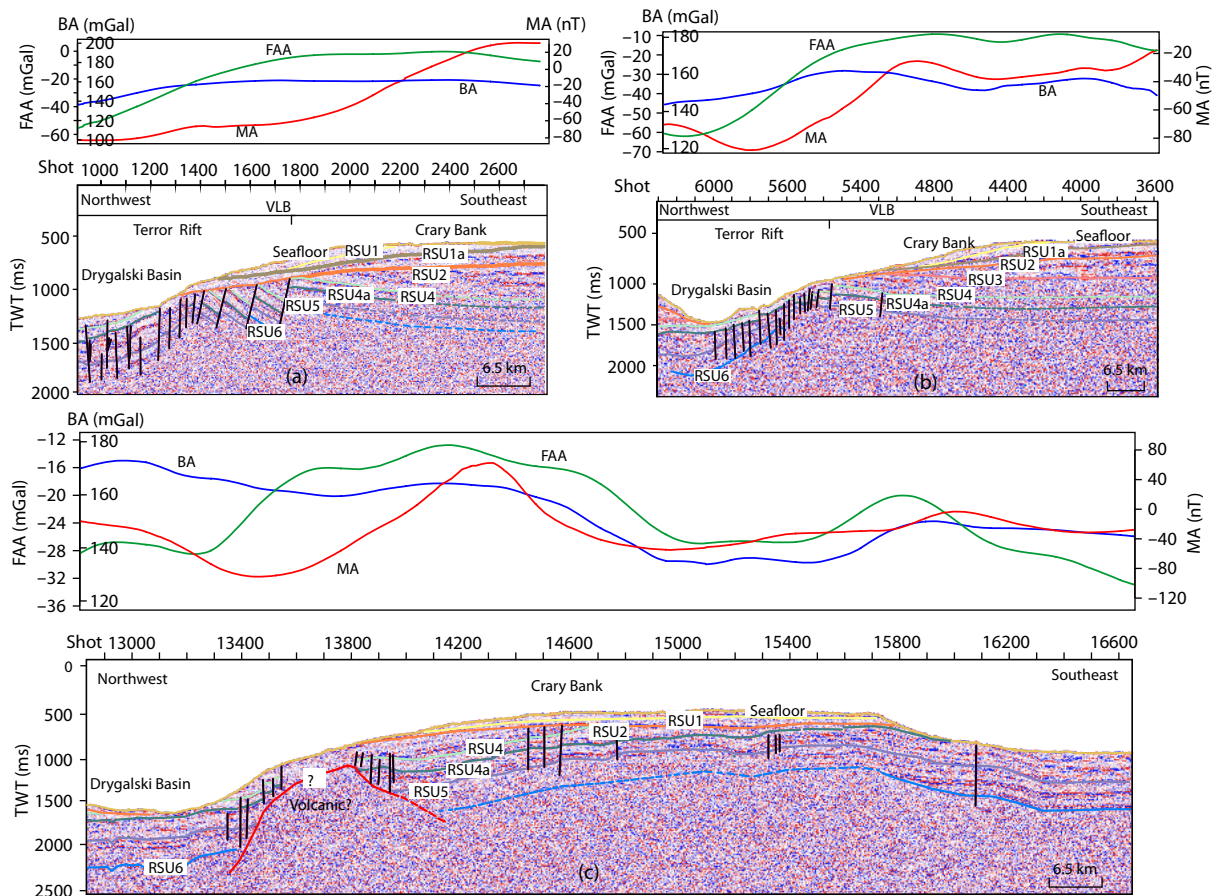


Figure 4. The magnetic and gravity anomalies of CHINARE seismic profiles. (a) Profile ANT32-L01 passes through the Terror Rift. (b) ANT32-L03 passes through the Terror Rift and cuts part of the Crary Bank. The strata above RSU6 appear only in the Terror Rift, and above RSU4, they are severely denuded. (c) ANT32-L09 passes through the VLB and the Coulman High and enters into the Central Basin. The chaotic reflection has a length of approximately 16 km (shot number: 13300–13800), generally located at the junction of the VLB and Coulman High. Unconformity RSU6 may represent the basement of the Coulman High and is covered by multiples. FAA, free-air gravity anomaly; BA, Bouguer gravity anomaly; MA, magnetic anomaly; TWT, two-way travel time.

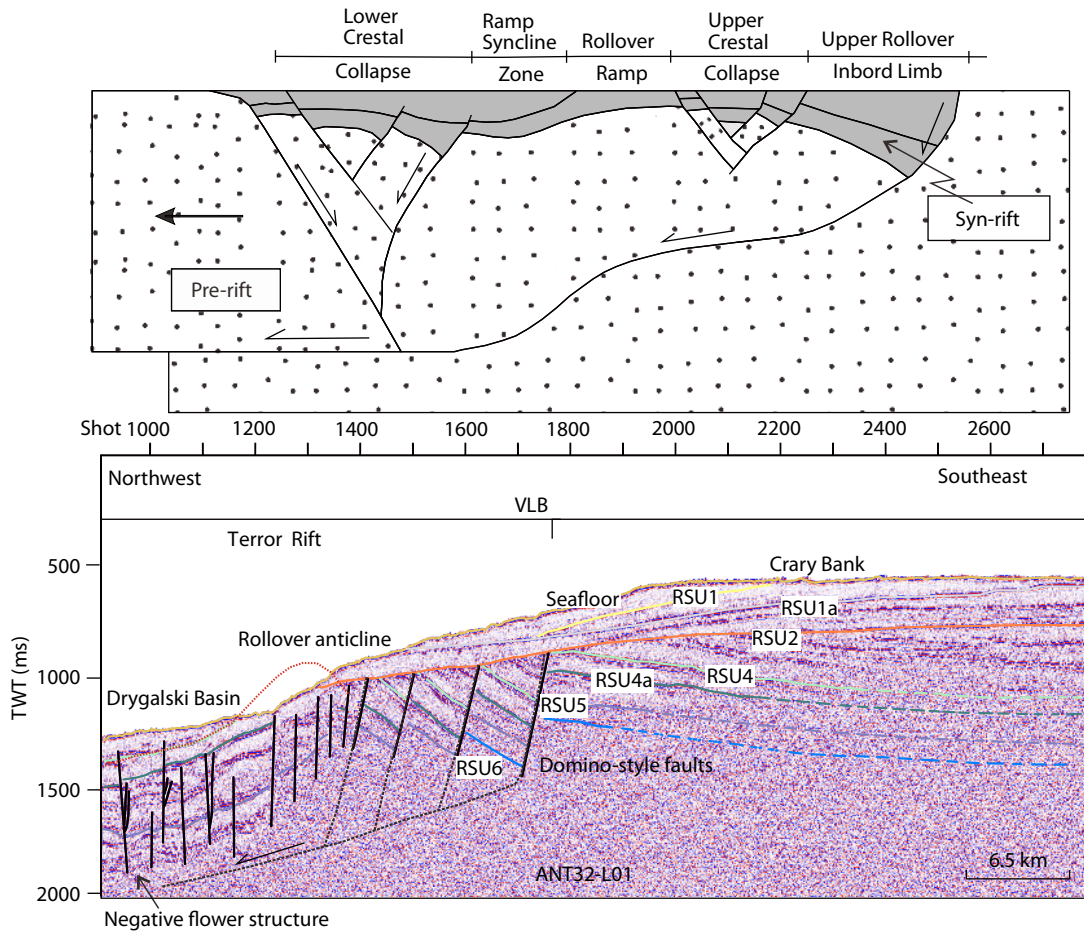


Figure 5. Schematic diagram of the rollover anticline in the Terror Rift. The rollover model above is from McClay (1995). The red dotted line represents the structure of the restored anticline of unconformity RSU4.

enced strike-slip motion between 18 and 24 Ma to form oblique tension, resulting in accommodation zones. North-south trending faults turn to be northwest-southeast trending, forming dextral offsets of ~25 km (Salvini et al., 1997). Profile ANT32-L01 intersects with the Campbell Fault and the Priestley Fault, indicating that the negative flower structure here could have been directly affected by the dextral strike-slip fault. Therefore, the negative flower structures found in profile ANT32-L01 support the interpretation of an accommodation zone.

A rollover anticline forms an uplift in profile ANT32-L01. The strata of ANT32-L01 between RSU4 and RSU2 are staggered by domino-style faults with similar strikes and dips. These faults may have been formed in the same period and may be shallow parts of a detachment fault, representing the eastern boundary of the Terror Rift. Faults, however, were truncated above RSU2 (~4.6 Ma) in the Lee Arch, and the sedimentary thicknesses between RSU6 and RSU4 are uniform. Strata have been uplifted in the northern Terror Rift and are eroded at RSU2 (~4.6 Ma), indicating that the uplift occurred earlier than 4.6 Ma and that a part of the Lee Arch was formed by a rollover anticline (Figure 5; McClay, 1995; Hall et al., 2007). When in a tensional setting, the hanging wall of a fault is pulled apart from the footwall, forming a potential accommodation space. Under gravitational forces, the collapsed hanging wall bends and deforms, and a rollover anticline is formed. The pre-

conditions for a rollover anticline are as follows: the existence of an anticline, slope syncline, and top collapse; no large strip of volcanic intrusion perpendicular to the structural direction (confirmed by gravity and magnetic anomaly data); an existing initial detachment fault (McClay, 1995). All these conditions are met in profile ANT32-L01. Therefore, the domino-style faults form a large detachment surface, resulting in the strata tilt and the formation of the rollover anticline in the northern Terror Rift.

Profile ANT32-L09 (Figure 4) passes through the VLB and Crary Bank but is located outside the Terror Rift. A chaotic reflection zone of approximately 16 km wide is located on the western side of the Crary Bank, where secondary faults rose to the seabed and may be related to dextral strike-slip faults from NVL. Besides the rollover anticline, it is unknown whether the structural uplifts in ANT32-L01 and ANT32-L03 came from the Terror Rift shoulder uplift. It is unclear whether the chaotic reflections of ANT32-L09 are similar to those from the previous two seismic profiles or whether they belong to volcanic structures.

4. Joint Interpretation of Gravity, Magnetic, and Seismic Data

The Discovery Graben in the Terror Rift has thick strata necessary for developing mud volcanoes. Mud volcanoes are mostly in the shape of mounds and are formed by the accumulation of intermit-

tently erupting mud and gas. Seismic profiles IT90AR-63S and IT90AR-65S pass through mud volcanoes in the Terror Rift (Figure 2; Geletti and Busetti, 2011). The tops of the mud volcanoes are roughly circular mounds with an average diameter of about 200–500 m and a depth of 30 m (Lawver et al., 2007). The region of mud volcanoes shows roughly negative free-air gravity and negative magnetic anomalies. The BSRs correspond to low magnetic anomalies and the mounds correspond to high magnetic anomalies (Figure 6). Mud volcanoes in the Terror Rift may have originated from volcanoes that erupted under an ice sheet during a reversal of the geomagnetic field, forming a hyaloclastite edifice (Lawver et al., 2012).

Along seismic profile NBP0401-148 (Figure 7a), the Lee Arch corresponds to a low magnetic anomaly, and high free-air and Bouguer gravity anomaly. These data imply that the Lee Arch may be a fold formed by a rollover anticline rather than by volcanism (Salvini et al., 1997; Hall et al., 2007).

Profile NBP9407-51 (Figure 7b) in the southern Terror Rift shows a volcanic intrusion that pierced through unit Rv (corresponding to RSU2, ~4.6 Ma; Henrys et al., 2008) and caused secondary faults. The volcanic intrusion may extend northward from Beaufort Island in the Lee Arch. The ages of dredged samples from Beaufort Island (Figure 8) range from 6.8 to 90 ± 5 ka (Rilling et al., 2009), younger than the Melbourne and Erebus Volcanic Provinces at the geographic endpoints of the Terror Rift. The independent intrusion in NBP9407-51, located on the west side of Franklin Island and north of Beaufort Island, may belong to the McMurdo Volcanic Group. Along the NBP9407-51, the volcanic intrusion corresponds to both high magnetic and high free-air gravity anomalies, different from the mud volcanoes analyzed above (Figure 6).

Profile L284AN-407 passes through the mud volcano area. Numerous mounds formed a rugged surface with short-wavelength, high-amplitude magnetic anomalies, indicating that the mud volcanoes have magnetic nuclei related to volcanic origin (Lawver et al., 2012). The eruptive volcanoes of L284AN-407 are on the Franklin Island, same as the intrusive volcano on profile NBP9407-51, with high magnetic and free-air gravity anomalies.

Profiles ANT32-L01 and ANT32-L03 show the uplift at the margin of the Terror Rift (Figure 4). The stratigraphic sequence has a high continuity, and faults reach the seafloor, indicating that the Terror Rift is still active. The gravity and magnetic anomalies are similar to those of profile NBP0401-148 and are in good agreement with the topography. The Bouguer gravity anomaly tends to be flat, suggesting that the uplifts in the two seismic profiles did not belong to the rift shoulder but were formed by the rollover anticline (Figure 5), because the rift is too young to have achieved gravity equilibrium for a shoulder uplift.

The chaotic reflection zone of ANT32-L09 (Figure 4), approximately 16 km in width, is located inside the VLB. The seismic profile is near a magnetic body that is linked to the southern McMurdo Volcanic Group, the Erebus Province, but is unrelated to a large-scale igneous intrusion at 48–34 Ma between the Northern Basin and the VLB (Polar-3; Figure 2c). Firstly, the axial direction of the high magnetic body is not parallel to that of Polar-3. However, the axial direction is perpendicular to the east-west extension caused by dextral strike-slip faults from NVL, indicating that a high magnetic anomaly was generated along the weak zone. Secondly, profile ANT32-L09 passes through the high magnetic body and shows a chaotic reflection. The chaotic reflection is younger than RSU2 (~4.6 Ma) and may correspond to the strong Neogene volcanism of the McMurdo Volcanic Group in the southern VLB. Thirdly, the gravity and magnetic anomalies of the chaotic reflection are consistent with the features of some volcanoes, such as those on the Beaufort Island.

The free-air gravity anomaly above the chaotic reflection area is higher than that in Coulman High (Figure 4). The magnetic anomaly curve of ANT32-L09 (Figure 4) has two peaks corresponding to one high free-air gravity anomaly, suggesting that the underground structure with a negative magnetization may belong to a unit with a different tectonic activity. Coincidentally, some volcanoes in the southern Terror Rift have undergone two eruptions with opposite magnetization, such as those on the Beaufort Island (6.77–6.80 Ma; Rilling et al., 2009). Through an analysis of dredged samples, we found that the magnetic anomalies in the west wing are negative, whereas those in the east wing are positive.

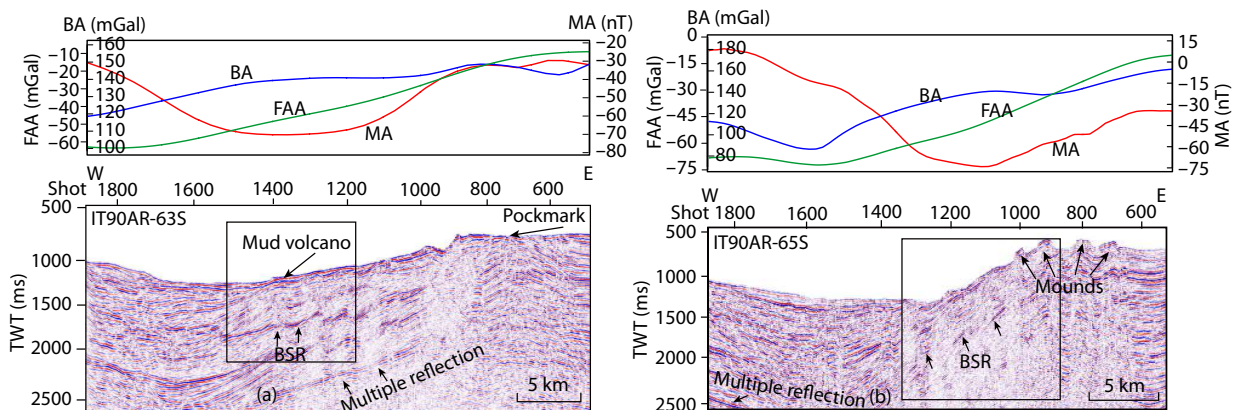


Figure 6. Characteristics of gravity and magnetic anomalies along the studied seismic profiles. (a) IT90AR-63S; (b) IT90AR-65S. The black box shows bottom-simulating reflectors (BSRs). Seafloor pockmark and mud volcanoes are shown on the seismic profiles (Geletti and Busetti, 2011). FAA, free-air gravity anomaly; BA, Bouguer gravity anomaly; MA, magnetic anomaly; TWT, two-way travel time.

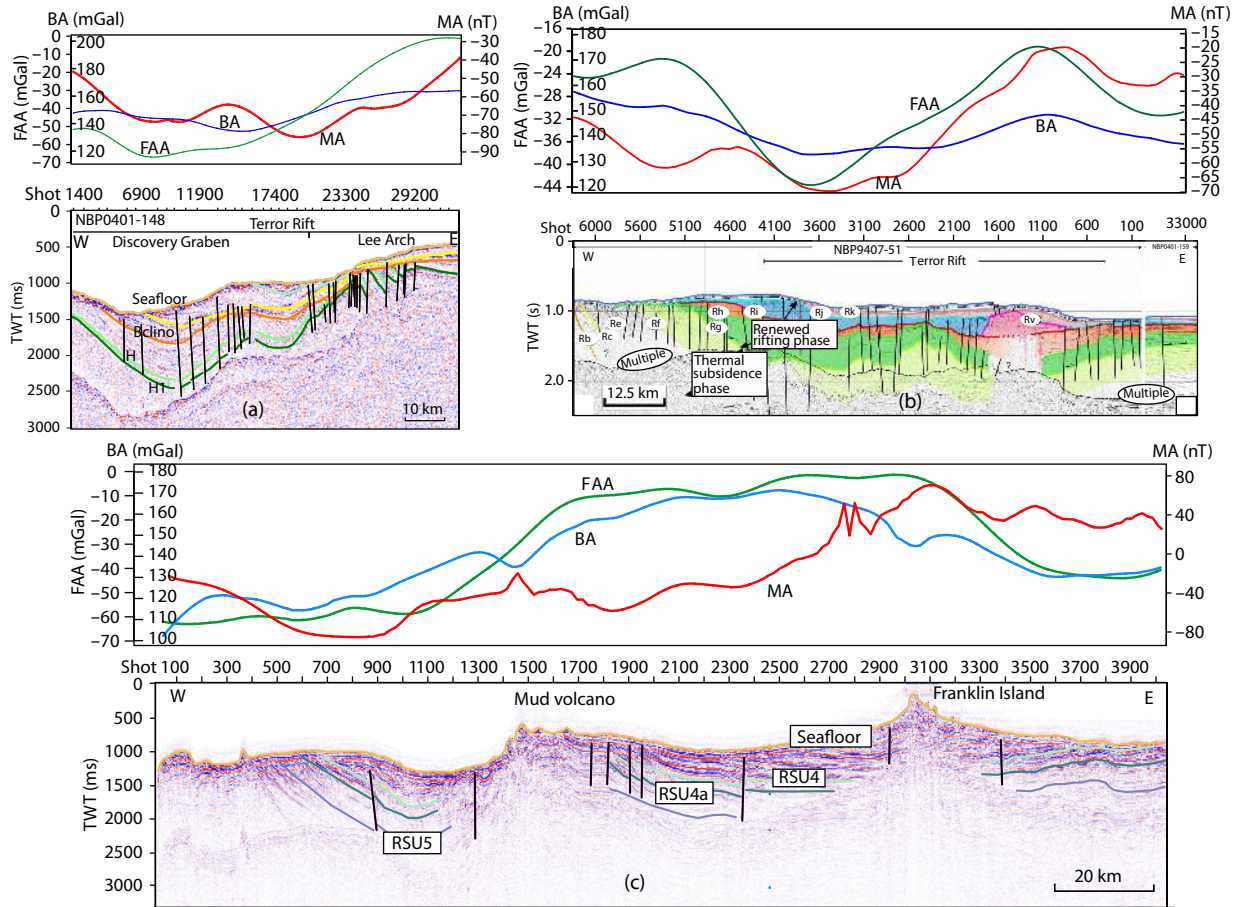


Figure 7. Characteristics of gravity and magnetic anomalies along with the studied seismic profiles. (a) NBP0401-148 is after Hall et al. (2007). The seismic horizon is based on ANDRILL (Fielding et al., 2006), in which H1 may correspond to RSU4a, H corresponds to RSU4, and Bclino corresponds to erosion interface RSU2. (b) NBP9407-51 is after Henrys et al. (2008). The profile passes through the southern Terror Rift, and Rv, corresponding to RSU2 (~4.6 Ma), is the top of the volcanic intrusion. Units Rb–Rf are made by early rifting (~34–29 Ma), the ages of units Rf–Rk are referred to Figure 3, and Rv is related to volcanism (~2.8 Ma). (c) L284AN-407 passes through mud volcanoes located inside the Terror Rift and Franklin Island. FAA, free-air gravity anomaly; BA, Bouguer gravity anomaly; MA, magnetic anomaly; TWT, two-way travel time.

ive (Figure 9). The opposite magnetic anomalies are similar to those of the chaotic reflection area on ANT32-L09. The intrusion of NBP9407-51 shows a strong positive magnetic anomaly. The ages of these two features are consistent with the formation under opposite geomagnetic polarities.

Between 6.57 and 6.94 Ma, the geomagnetic field may have been in negative polarity (Cande and Kent, 1995), so the strong negative magnetic characteristics would have been preserved rapidly in the VLB during this period. If a large amount of volcanic eruptions had occurred prior to 6.94 Ma or younger than 6.57 Ma, the overall magnetic anomaly of this feature would be positive. The dredged sample of Beaufort Island is between 6.77 and 6.80 Ma, recording a rapid emplacement of the igneous rocks during the negative polarity. A positive magnetic anomaly observed on the southwest side of the island represents a younger intrusion that may have cooled after 6.57 Ma (Rilling et al., 2009), indicating that Beaufort Island had at least two eruptions with opposite geomagnetism.

Similarly, the Franklin Island on profile L284AN-407 is younger than 3.7 Ma (~3.2–3.7 Ma) and shows a positive magnetic anom-

aly in the normal polarity between 3.33 and 3.58 Ma (Cande and Kent, 1995). Therefore, the intrusion identified on ANT32-L09 is younger than 4.6 Ma and may have been formed in two or more different periods of volcanism. Profile ANT32-L09 did not penetrate deeply enough to define the depth and scope of the intrusion, but it shows a trend of eastward extension. A longer period of negative polarity between 3.58 and 4.18 Ma (Cande and Kent, 1995) could help date the intrusion, which shows a negative magnetic anomaly.

5. Discussion

The east-west extension of the VLB is affected by the dextral strike-slip faults in the NVL, and the latest extension forms the Terror Rift, which is spatially limited by the Neogene igneous provinces. Under these influences, volcanism occurs frequently. To study the distribution of volcanism in the VLB, MCS profiles from south to north were selected. Mud volcanoes on profiles IT90AR-63S, L284AN-407, and IT90AR-65S were concentrated in the middle of the Terror Rift (Figure 2). The gravity and magnetic anomaly anomalies showed that mud volcanoes with short-wavelength positive or negative magnetic anomalies may be re-

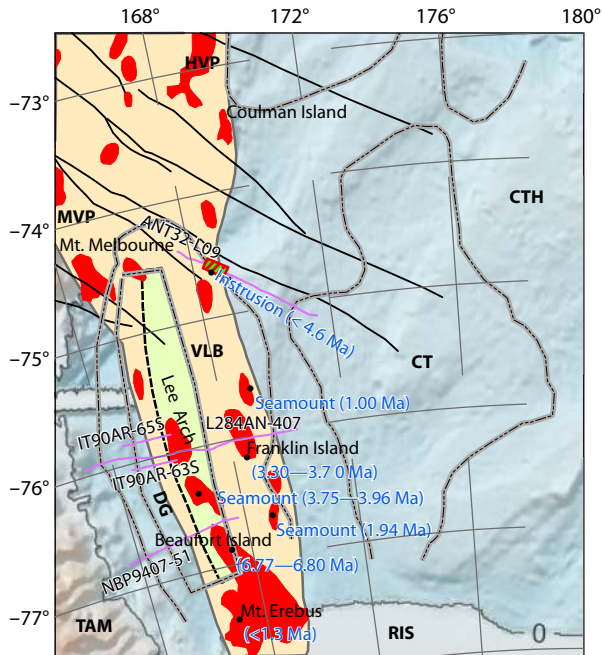


Figure 8. Volcanic distributions map (after Salvini et al., 1997). The gray dash-dotted lines represent structural blocks. The thick black lines are dextral strike-slip faults, which are the same as in Figure 1. The yellow area is the brittle volcanic region (Salvini et al., 1997), the red areas are volcanoes, and the yellow striped red square is the chaotic reflection area in ANT32-L09. The enclosed rectangle in green on the east side of the Terror Rift is the Lee Arch, and DG is the Discovery Graben. The ages of volcanoes were estimated from analysis of the petrochemical evidence and interpretation of the seismic data. VLB, Victoria Land Basin; CT, Central Trough; CTH, Central High; RIS, Ross Ice Shelf; TAM, Transantarctic Mountains.

lated to magmatic volcanism. Most magmatic volcanoes have magnetic anomalies of opposite polarization in the VLB, which indicates multi-stages of volcanism since the Neogene. Profiles ANT32-L01 and ANT32-L03 in the northern Terror Rift show a rollover anticline, leading to the uplift of the Lee Arch. The thick sediments on the western Terror Rift favor oil and gas resources, and the high-angle normal faults developed on the Lee Arch can provide channels for oil and gas migration or volcanic activities.

The volcanic intrusions on profile ANT32-L09, showing high free-air gravity and strong magnetic anomalies, underwent multi-stages of volcanism. In addition, magmatic volcanoes on Franklin Island in L284AN-407 and Beaufort Island in NBP9407-51 showed high free-air gravity and magnetic anomalies, respectively. The ages and geophysical characteristics attest to the fact that the magmatic intrusions and the volcanoes belong to the McMurdo Volcanic Group. From the gravity and magnetic anomalies in the Ross Sea Basin, the volcanoes on the east side of the VLB seem to be parallel to the north-south trend of the Terror Rift. Therefore, volcanoes inside the Terror Rift occur along the trend of the Lee Arch, and those outside the Terror Rift are approximately parallel to each other, forming two volcanic chains from north to south. We suggest that the two volcanic chains connect the three large igneous provinces, because the geophysical characteristics of the

western Ross Sea are consistent with the distribution of the two chains, and geochemical evidence suggests that they are of similar ages. Along with multiple extensions in the VLB, sometimes volcanism surged up in the weak zone to have formed a brittle volcanic region with high free-air and Bouguer gravity anomalies and strong magnetic anomalies.

The two volcanic chains may be related to a change in the crustal rheology in the VLB. The Moho becomes shallow from 35 to 40 km under the TAM to 18–20 km in the Ross Sea Basin (Cooper, 1989), and the brittle volcanic region in the VLB likely formed through intense volcanic activities. The deformation of the brittle volcanic region provided favorable permeability conditions for the magmatic intrusion. Dextral strike-slip faults with different rheology patterns and crust thicknesses pass through the VLB. The VLB extension and the strike-slip faulting together form a northwest-southeast fracture zone—the brittle volcanic region in the VLB (Salvini et al., 1997). The western side of the brittle volcanic region seems to be limited by the Lee Arch, and the eastern side extends roughly to the VLB (Figure 8). Bathymetric, topographic, and seismic data show that the magmatic volcanoes in the Lee Arch are nearly north-south in orientation and that they connect to Mt. Erebus and Mt. Melbourne.

On the eastern flank of the VLB, a series of magmatic volcanoes and volcanic intrusions are exposed near the Franklin Island with narrow and long clusters. Farther north, the volcanic intrusion on profile ANT32-L09 is 16 km wide, with a newborn volcanic edifice protruded from the strongly eroded seabed and the boundary of the Coulman High. Simultaneously, according to the age and geophysical characteristics, the volcanic intrusion found on ANT32-L09 is Neogene in age, consistent with the McMurdo Volcanic Group in the south. The western boundary of the brittle volcanic region runs along the Lee Arch, but whether it connects to Mt. Melbourne has not been determined, due to severe erosion by multiple glaciations and sparse seismic data. Glacial erosion may have weakened the fault activities in the northern VLB and removed the volcanic record. The uplift of the sedimentary unit in the Lee Arch makes it possible for younger magmatic volcanism to emplace along the bottom fault. The Neogene magmatic volcanoes are exposed on Beaufort Island. Near the island, magmatic volcanic clusters include mud volcanoes with magnetic nuclei.

The samples dredged in the VLB show that the volcanic eruption is younger than 8 Ma, and that the volcanic intrusions located in NBP9407-51 and ANT32-L09 are younger than 4.6 Ma (piercing the RSU2 unconformity). Although the age distributions are nonuniform (Figure 8), magmatic volcanism began after the formation of the Terror Rift. On the gravity and magnetic anomaly maps of the Ross Sea Basin (Figure 2), relatively continuous high magnetic anomalies were observed in the VLB, connecting the high anomalies at the north and south ends. The high Bouguer anomalies also showed a nearly north-south trend in the VLB, which is consistent with the range of the brittle volcanic region.

6. Conclusions

This study helps explain the dynamic behaviors of the Terror Rift and the temporal and spatial distributions of tectonic activities in the VLB. The high-resolution seismic stratigraphic sequences of

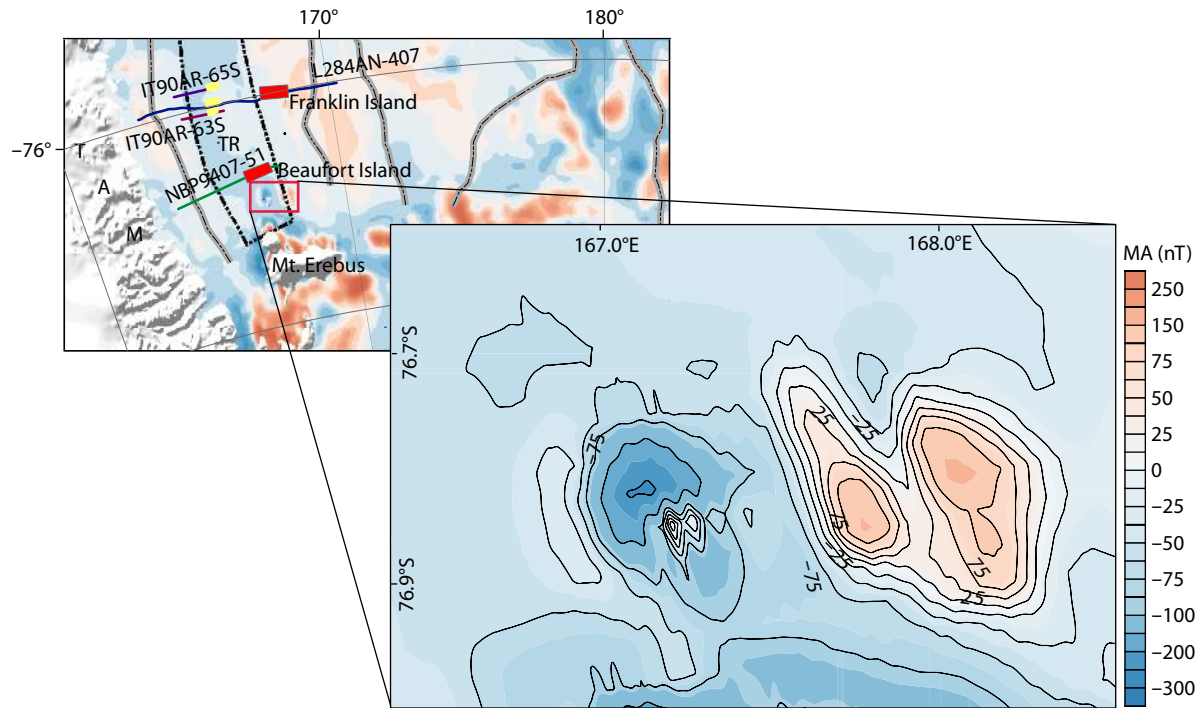


Figure 9. Magnetic anomalies (MA) of the Beaufort Island. The volcanos first erupted during negative polarity and then erupted during normal polarity.

the CHINARE profiles were calibrated by the DSDP 273 to interpret the sedimentary structure in the northern Terror Rift. The negative flower structures and rollover anticlines indicate that the northern Terror Rift was affected by northwest-southeast strike-slip faults and north-south detachment faults. The flower structures are not fully developed in the Discovery Graben formed between 24 and 18.38 Ma. In addition to the accommodation zone of the Terror Rift, we can infer that the Terror Rift transited from orthogonal to oblique tension from 24 to 18.38 Ma. The Lee Arch may be related to the rollover anticline formed by the detachment fault and may provide channels for magmatic volcanism.

Under the impact of the northwest-southeast trending right-lateral strike-slip fault and the extension of the north-south trending basin, the VLB may have been deformed and become part of the brittle volcanic region. Magma flowed easily at the intersection of faults, forming two north-south trending volcanic chains, which limited the boundary of the brittle volcanic region. The eastern chain of volcanoes connects the Erebus Province on Ross Island, the intrusion feature on ANT32-L09, and the Hallett Volcanic Province on northern Coulman Island. The western chain of volcanoes connects the Erebus Volcanic Province on Ross Island, mud volcanoes, and the Melbourne Volcanic Province around Mt. Melbourne. The magmatic volcanoes belong to the Neogene McMurdo Volcanic Group and have undergone multiple eruptions. We speculate that the chains will help study the three igneous provinces in the future. In this work, we questioned the traditional extension mechanism of the Terror Rift and systematically summarized the distribution of volcanism in the VLB.

Acknowledgments

This research was supported by the Impact and Response of Ant-

arctic Seas to Climate Change Project (IRASCC01-03-01), Hainan Natural Science Foundation Innovative Research Team Project (421CXDT441), and the National Natural Science Foundation of China (Nos. 42176067, 41576069, 42176055, 41776189 and 41906197). We thank the 32nd CHINARE and the Antarctic Seismic Data Library System of SCAR (SDLS; <http://sdlsold.ogs.trieste.it>) for the MCS data available. We thank two anonymous reviewers whose comments and suggestions helped improve this manuscript.

References

- Bayasgalan, A., Jackson, J., Ritz, J. F., and Carretier, S. (1999). 'Forebergs', flower structures, and the development of large intra-continental strike-slip faults: The Gurvan Bogd fault system in Mongolia. *J. Struct. Geol.*, 21(10), 1285–1302. [https://doi.org/10.1016/S0191-8141\(99\)00064-4](https://doi.org/10.1016/S0191-8141(99)00064-4)
- Blocher, W. B. (2017). *Fault Geometry and Kinematics within the Terror Rift, Antarctica*. The Ohio State University.
- Brancolini, G., Busetti, M., Marchetti, A., De Santis, L., Zanolla, C., Cooper, A. K., Cochran, G. R., Zayatz, I., Belyaev, V., Hinz, K. (1995). Descriptive text for the seismic stratigraphic atlas of the Ross Sea, Antarctica. In A. K. Cooper, et al. (Eds.), *Geology and Seismic Stratigraphy of the Antarctic Margin* (pp. A271–A286). Washington, DC: American Geophysical Union. <https://doi.org/10.1002/9781118669013.app1>
- Cande, S. C., and Kent, D. V. (1995). Revised calibration of the geomagnetic polarity timescale for the Late Cretaceous and Cenozoic. *J. Geophys. Res.: Solid Earth*, 100(B4), 6093–6095. <https://doi.org/10.1029/94JB03098>
- Cooper, A. K., Davey, F. J., and Behrendt, J. C. (1987). Seismic stratigraphy and structure of the Victoria Land Basin, western Ross Sea, Antarctica. In A. K. Cooper, et al. (Eds.), *The Antarctic Continental Margin: Geology and Geophysics of the Western Ross Sea* (pp. 27–77). Houston: Circum-Pacific Council for Energy and Resources.
- Cooper, A. K. (1989). Crustal structure of the Ross Embayment, Antarctica. In H. T. Huh, et al. (Eds.), *Proceedings of 1st International Symposium on Antarctic Science* (pp. 57–72). Seoul: Korea Ocean Research and Development

- Institute.
- Davey, F. J., and Santis, L. D. (2006). A multi-phase rifting model for the Victoria Land Basin, western Ross Sea. In D. K. Fütterer, et al. (Eds.), *Antarctica* (pp. 303–308). Berlin: Springer. https://doi.org/10.1007/3-540-32934-X_38
- Fielding, C. R., Henrys, S. A., and Wilson, T. J. (2006). Rift history of the western Victoria Land Basin: A new perspective based on integration of cores with seismic reflection data. In D. K. Fütterer, et al. (Eds.), *Antarctica* (pp. 309–318). Berlin: Springer. https://doi.org/10.1007/3-540-32934-X_39
- Fielding, C. R., Whittaker, J., Henrys, S. A., Wilson, T. J., and Naish, T. R. (2008). Seismic facies and stratigraphy of the Cenozoic succession in McMurdo Sound, Antarctica: Implications for tectonic, climatic and glacial history. *Palaeogeogr., Palaeoclimatol., Palaeoecol.*, 260(1–2), 8–29. <https://doi.org/10.1016/j.palaeo.2007.08.016>
- Fielding, C. R. (2018). Stratigraphic architecture of the Cenozoic succession in the McMurdo Sound region, Antarctica: An archive of polar palaeoenvironmental change in a failed rift setting. *Sedimentology*, 65, 1–61. <https://doi.org/10.1111/sed.12413>
- Geletti, R., and Busetti, M. (2011). A double bottom simulating reflector in the western Ross Sea, Antarctica. *J. Geophys. Res.: Solid Earth*, 116(B4), B04101. <https://doi.org/10.1029/2010JB007864>
- Golynsky, A., Chiappini, M., Damaske, D., Ferraccioli, F., Finn, C. A., Ishihara, T., Kim, H. R., Kovacs, L., Masolov, V. N., von Frese, R. (2006). ADMAP—A digital magnetic anomaly map of the Antarctic. In D. K. Fütterer, et al. (Eds.), *Antarctica* (pp. 109–116). Berlin: Springer. https://doi.org/10.1007/3-540-32934-X_12
- Hall, J., Wilson, T., and Henrys, S. (2007). Structure of the central Terror Rift, western Ross sea, Antarctica. In A. Cooper, et al. (Eds.), *Antarctica: A Keystone in a Changing World—Online Proceedings of the 10th ISAES*. Open-File Report 2007-1047. Reston, Virginia: U.S. Geological Survey.
- Harry, D. L., and Anoka, J. (2007). Geodynamic models of the tectonomagmatic evolution of the West Antarctic Rift System. In A. Cooper, et al. (Eds.), *Antarctica: A Keystone in a Changing World—Online Proceedings of the 10th ISAES*. Open-File Report 2007-1047. Reston, Virginia: U.S. Geological Survey.
- Hayes, D. E., Frakes, L. A., Barrett, P. J., Burns, D. A., Chen, P. H., Ford, A. B., and Kaneps, A. G. (1975). *Initial Reports of the Deep Sea Drilling Project, Volume 28* (pp. 335–367). Washington U.S. Government Printing Office.
- Henrys, S., Wilson, T., Whittaker, J. M., Fielding, C., Hall, J., and Naish, T. (2008). Tectonic history of mid-Miocene to present southern Victoria Land Basin, inferred from seismic stratigraphy in McMurdo Sound, Antarctica. In A. Cooper, et al. (Eds.), *Antarctica: A Keystone in a Changing World—Online Proceedings of the 10th ISAES*. Open-File Report 2007-1047. Reston, Virginia: U.S. Geological Survey.
- Ji, F., Gao, J. Y., Li, F., Shen, Z. Y., Zhang, Q., and Li, Y. D. (2017). Variations of the effective elastic thickness over the Ross Sea and Transantarctic Mountains and implications for their structure and tectonics. *Tectonophysics*, 717, 127–138. <https://doi.org/10.1016/j.tecto.2017.07.011>
- Kooyman, G. L., Goetz, K., Williams, C. L., Ponganis, P. J., Sato, K., Eckert, S., Horning, M., Thorson, P. T., and Van Dam, R. P. (2020). Cray bank: A deep foraging habitat for emperor penguins in the western Ross Sea. *Polar Biol.*, 43(7), 801–811. <https://doi.org/10.1007/s00300-020-02686-3>
- Kyle, P. R., and Cole, J. W. (1974). Structural control of volcanism in the McMurdo Volcanic Group, Antarctica. *Bull. Volcanol.*, 38(1), 16–25. <https://doi.org/10.1007/BF02597798>
- Kyle, P. R. (1990). A. McMurdo volcanic group western Ross embayment. In W. E. LeMasurier, et al. (Eds.), *Volcanoes of the Antarctic Plate and Southern Oceans, Volume 48* (pp. 18–145). Washington, DC: American Geophysical Union. <https://doi.org/10.1029/AR048p0018>
- Lawver, L., Lee, J., Kim, Y., and Davey, F. (2012). Flat-topped mounds in western Ross Sea: Carbonate mounds or subglacial volcanic features?. *Geosphere*, 8(3), 645–653. <https://doi.org/10.1130/GES00766.1>
- Lawver, L. A., Davis, M. B., Wilson, T. J., and Shipboard Scientific Party. (2007). Neotectonic and other features of the Victoria Land Basin, Antarctica, interpreted from multibeam bathymetry data. In A. Cooper, et al. (Eds.), *Antarctica: A Keystone in a Changing World—Online Proceedings of the 10th ISAES*. Open-File Report 2007-1047. Reston, Virginia: U.S. Geological Survey.
- Magee, W. R. (2011). *Magnitude of Extension Across the Central Terror Rift, Antarctica: Structural Interpretations and Balanced Cross Sections*. Columbus, Ohio: The Ohio State University.
- Massironi, M., and Kim, Y. S. (2014). Strike-slip faults. In *Encyclopedia of Planetary Landforms* (pp. 1–12). New York: Springer. https://doi.org/10.1007/978-1-4614-9213-9_548-1
- McClay, K. R. (1995). 2D and 3D analogue modelling of extensional fault structures; templates for seismic interpretation. *Petrol. Geosci.*, 1(2), 163–178. <https://doi.org/10.1144/petgeo.1.2.163>
- Pappa, F., Ebbing, J., and Ferraccioli, F. (2019). Moho depths of Antarctica: Comparison of seismic, gravity, and isostatic results. *Geochem., Geophys., Geosyst.*, 20(3), 1629–1645. <https://doi.org/10.1029/2018GC008111>
- Rilling, S., Mukasa, S., Wilson, T., Lawver, L., and Hall, C. (2009). New determinations of ⁴⁰Ar/³⁹Ar isotopic ages and flow volumes for Cenozoic volcanism in the Terror Rift, Ross Sea, Antarctica. *J. Geophys. Res.: Solid Earth*, 114(B12), B12207. <https://doi.org/10.1029/2009JB006303>
- Rossetti, F., Storti, F., Busetti, M., Lisker, F., Di Vincenzo, G., Läufer, A. L., Rocchi, S., and Salvini, F. (2006). Eocene initiation of Ross Sea dextral faulting and implications for East Antarctic neotectonics. *J. Geol. Soc.*, 163(1), 119–126. <https://doi.org/10.1144/0016-764905-005>
- Salvini, F., Brancolini, G., Busetti, M., Storti, F., Mazzarini, F., and Coren, F. (1997). Cenozoic geodynamics of the Ross Sea region, Antarctica: Crustal extension, intraplate strike-slip faulting, and tectonic inheritance. *J. Geophys. Res.: Solid Earth*, 102(B11), 24669–24696. <https://doi.org/10.1029/97JB01643>
- Salvini, F., and Storti, F. (1999). Cenozoic tectonic lineaments of the Terra Nova Bay region, Ross embayment, Antarctica. *Global Planet. Change*, 23(1–4), 129–144. [https://doi.org/10.1016/S0921-8181\(99\)00054-5](https://doi.org/10.1016/S0921-8181(99)00054-5)
- Sandwell, D. T., Müller, R. D., Smith, W. H. F., Garcia, E., and Francis, R. (2014). New global marine gravity model from CryoSat-2 and Jason-1 reveals buried tectonic structure. *Science*, 346(6205), 65–67. <https://doi.org/10.1126/science.1258213>
- Sauli, C., Sorlien, C., Busetti, M., De Santis, L., Geletti, R., Wardell, N., and Luyendyk, B. P. (2021). Neogene development of the terror rift, Western Ross Sea, Antarctica. *Geochem., Geophys., Geosyst.*, 22(3), e2020GC009076. <https://doi.org/10.1029/2020GC009076>
- Shapiro, N. M., and Ritzwoller, M. H. (2004). Inferring surface heat flux distributions guided by a global seismic model: Particular application to Antarctica. *Earth Planet. Sci. Lett.*, 223(1–2), 213–224. <https://doi.org/10.1016/j.epsl.2004.04.011>
- Talarico, F. M., and Sandroni, S. (2011). Early Miocene basement clasts in ANDRILL AND-2A core and their implications for paleoenvironmental changes in the McMurdo Sound region (western Ross Sea, Antarctica). *Global Planet. Change*, 78(1–2), 23–35. <https://doi.org/10.1016/j.gloplacha.2011.05.002>
- Trey, H., Cooper, A. K., Pellis, G., Della Vedova, B., Cochrane, G., Brancolini, G., and Makris, J. (1999). Transect across the West Antarctic rift system in the Ross Sea, Antarctica. *Tectonophysics*, 301(1–2), 61–74. [https://doi.org/10.1016/S0040-1951\(98\)00155-3](https://doi.org/10.1016/S0040-1951(98)00155-3)
- Xu, Z., Gao, J. Y., Yang, C. G., and Shen, Z. Y. (2018). A new high-resolution digital bathymetric model of the Ross Sea, Antarctica. *Chin. J. Polar Res. (in Chinese)*, 30(4), 360–369. <https://doi.org/10.13679/j.jdyj.20180011>